

Localization of the Center Region of Highest Muscle Spindle Abundance in Posterior Forearm Muscles for Botulinum Toxin Injection

Localización de la Región Central de Mayor Abundancia de Husos Musculares en los Músculos del Compartimiento Posterior del Antebrazo para la Inyección de Toxina Botulínica

Lin Xiang¹; Xia Wu¹; Jinjun Liu¹; Daihuan Luo¹; Ling Tao¹; Ming Xiaoming Zhang² & Shengbo Yang³

XIANG, L.; WU, X.; LIU, J.; LUO, D.; TAO, L.; ZHANG, M. X. & YANG, S. Localization of the center region of highest muscle spindle abundance in posterior forearm muscles for botulinum toxin injection. *Int. J. Morphol.*, 44(2):562-573, 2026.

SUMMARY: This study aimed to define the precise body surface puncture points and depths for the central region of highest muscle spindle abundance (CRHMSA) in posterior forearm muscles to guide botulinum toxin injections. In a study using 24 cadavers, we employed Sihler's staining for intramuscular nerves, histological quantification for muscle spindles, and computed tomography scanning for CRHMSA localization. Reference lines included the horizontal (H-line, between the humeral epicondyles) and longitudinal (L-line, from the lateral epicondyle to the radial styloid). The PP' line, representing puncture depth, was defined as the distance between the CRHMSA's anterior (P) and posterior (P') skin projections. The CRHMSA was located in the middle of the nerve-dense region (INDR) for the extensor carpi radialis longus, extensor carpi radialis brevis, extensor digitorum, extensor digiti minimi, abductor pollicis longus, extensor indicis, and supinator, and in the upper portion of the INDR for the extensor carpi ulnaris, extensor pollicis brevis, and extensor pollicis longus. The H-line coordinates were 14.67 %, 19.61 %, 10.66 %, 37.56 %, 25.75 %, 48.48 %, 39.51 %, 45.86 %, 33.40 %, and 50.80 %, respectively. L-line coordinates were 3.45 %, 39.50 %, 21.61 %, 44.20 %, 53.88 %, 86.39 %, 25.74 %, 37.67 %, 77.51 %, and 69.46 %, respectively. Puncture depths were 9.67 %, 6.52 %, 13.62 %, 10.35 %, 30.48 %, 14.99 %, 22.45 %, 12.65 %, 16.21 %, and 28.44 % of the PP' line, respectively. These findings provide anatomical guidance to enhance the accuracy of botulinum toxin injections for spasticity treatment.

KEY WORDS: Muscles of the compartment of forearm; Intramuscular nerve; Muscle spindle abundance; Botulinum toxin; Target localization.

INTRODUCTION

With the advancement of medicine, the survival rate of patients with central nervous system diseases such as stroke, traumatic brain injury, and spinal cord injury has significantly improved. However, there are about 65 % to 80 % of these patients experience secondary muscle spasms (Mahrous *et al.*, 2024; Therkildsen *et al.*, 2024). The symptoms of forearm posterior muscle spasm manifest as muscle stiffness and pain, occasionally accompanied by involuntary movement, which seriously affects daily life (Schnitzler *et al.*, 2022). In addition, lateral epicondylitis is commonly associated with elbow pain and often affects the extensor carpi ulnaris, extensor digiti minimi, extensor pollicis longus, and extensor carpi brevis (Galván Ruiz *et*

al., 2019; Poenaru *et al.*, 2024). Diseases such as Parkinson's disease and multiple sclerosis can also cause upper limb tremors, leading to functional impairments in drinking, eating, writing, and create social anxiety (Motavasseli *et al.*, 2024).

Botulinum toxin (BoNT) has become an effective treatment for muscle spasms, muscle tone disorders, and related pain by blocking the release of acetylcholine at the motor endplate (Yu *et al.*, 2023; Facciorusso *et al.*, 2024). However, due to difficulties in obtaining fresh specimens, the localization research of the motor endplate band of the forearm posterior group muscles is not yet sufficient.

¹Department of Clinical Medicine, Xinqu New Developing District, Zunyi Medical University, Zunyi, China.

²Center for Medical Education, Westlake University School of Medicine, Hangzhou, China.

³Department of Anatomy, Xinqu New Developing District, Zunyi Medical University, Zunyi, China.

FUNDING. Support from the National Natural Science Foundation of China (No: 32260217) and the Science and Technology Key Project of Guizhou (No: ZK-2022-056) and the Guizhou University Student Innovation Program (No: S202310661176).

Previous studies have shown that the intramuscular nerve-dense region (INDR), is located in the same position as the motor endplate and can serve as an alternative target for BoNT injection (Wang *et al.*, 2022; Ji *et al.*, 2025). Considering the large range of INDR, conventional multi-point high-dose injections into the INDR can easily cause side effects (Slawek *et al.*, 2005; Kroumpouzou *et al.*, 2021). Muscle spindles, functioning as allometric stretch receptors, play a crucial role in a-g loop regulation (Li *et al.*, 2021). However, the distribution of muscle spindles is uneven, with higher abundance within the INDR (Hesse *et al.*, 2001; Phadke *et al.*, 2013; Zhou *et al.*, 2024). Therefore, accurately locating the center of the region of the highest muscle spindle abundance (CRHMSA) in INDR is expected to achieve efficient blockade of the intrafusal muscle fibers by BoNT, along with reducing its impact on the extrafusal muscle fibers and improving the quality of rehabilitation.

The aim of this study is to anatomically locate the surface projection and the depth of CRHMSA in the posterior forearm muscle group in order to provide clinical guidance for BoNT injection therapy.

MATERIAL AND METHOD

Specimen and ethical approval. Overall, 24 adult cadavers [aged 35–75 (mean, 57.7 ± 11.5) years] were included in this study (12 male and 12 female). The donors had no history of neuromuscular diseases or upper limb deformities. The causes of death of these donors were cancer, heart disease, and accidents. The informed consent of all body donors was obtained from the body subjects/and or their legal guardians/next of kin. This study was conducted in accordance with the Helsinki Declaration of 1964 and its subsequent amendments. Specimen collection and related experiments were approved by the Ethics Committee of Zunyi Medical University (Approval Number: #2022–1–008, January 4th, 2022). For Sihler's staining, 12 specimens (from six male and six female individuals) were fixed with formalin. To avoid tissue deformation by formalin fixation and better characterize the native state, the remaining 12 fresh cadavers preserved by freezing (6 male and 6 female) were used for optimal target localization.

Gross anatomical observation and reference line design.

With the cadaver lying supine, a longitudinal incision was made between the medial epicondyle of the humerus and the ulnar styloid process, and two horizontal incisions were made at 5 cm above the line between the medial and lateral epicondyles of the humerus, and at the line connecting the radial and ulnar styloid processes. The skin and subcutaneous fat were turned laterally as a layer, and the radial nerve and its branches innervating the posterior forearm muscles were

separated and exposed to observe their location, quantity, and the presence or absence of vascular accompaniments at the nerve entry points. To facilitate the description of the spatial relationship between botulinum toxin (BoNT) block target and bony landmarks, two body surface reference lines were designed: the curved percutaneously line connecting the lateral epicondyle of the humerus (point a) and the medial epicondyle of the humerus (point b) was designated as the horizontal reference line H; the line connecting the lateral epicondyle of the humerus and the styloid process of the radius (point c) was designated as the longitudinal reference line L.

Modified Sihler's staining to determine the intramuscular nerve-dense region.

The posterior forearm muscle samples of 12 corpses fixed with formalin were collected and stained with modified Sihler's staining. The process was as follows: Depigmentation: placed in the leaching solution (3 % potassium hydroxide and 0.2 % hydrogen peroxide) for 3–4 weeks; Decalcification: transferred to Sihler's I solution (glacial acetic acid, glycerol and 1 % chloral hydrate volume ratio of 1:2:12) for 3–4 weeks; Staining: immersed in Sihler's II solution (Ehrlich hematoxylin, glycerol and 1 % chloral hydrate volume ratio of 1:2:12) for 4 weeks; Decolouration and neutralization: decolouration in Sihler's I solution for 2–20 hours, followed by neutralization in 0.05 % lithium carbonate solution for 2 hours; Transparency: transparent for 1 week in a gradient of alcohol at a concentration of 40 % to 100 %. After staining, the muscles were placed on the X-ray reading box according to the anatomical position to observe the distribution pattern of intramuscular nerves. The specific location of the intramuscular nerve dense area (INDR) in the muscle belly was measured using a vernier caliper.

H&E staining and muscle spindle abundance calculation.

Twelve fresh-frozen corpse samples were thawed, and the posterior forearm muscles were dissected and isolated. According to the results of Sihler's staining, each sample's corresponding INDR was divided into upper, middle and lower equal segments along the longitudinal axis. After weighing the tissues of each part, dehydration, paraffin embedding, continuous sequential cross-section (5 μm -thick slices) and H&E staining were performed in steps. The actual number of muscle spindles was counted under the microscope (Note: the muscle spindles appearing in the same position in the sequential section were counted only once). The predicted number of muscle spindles was calculated according to the formula published in the reference (predicted number of muscle spindles $\text{Sp}_n = 20.5m_n^{0.49}$, where m_n is muscle weight) (Banks, 2006). Muscle spindle abundance is expressed by dividing the actual number by the predicted number. By comparing the abundance of muscle spindles in

the upper, middle and lower parts of INDR, the region with the highest muscle spindle abundance was determined, which was the target area of spasmodic muscle nerve block.

Spiral CT localization of CRHMSA. The thawed fresh muscles, each matched the size of the muscles removed for muscle spindle staining, were put in place of the vacancies left. Medical barium sulfate powder mixed with 801 glue was injected into these muscles to label the location of CRHMSA. Then the muscles were sutured back layer by layer *in situ*. The 128-slice spiral CT (scanning parameters: 120 kV, slice thickness 1 mm, collimation 64×0.5 mm, pitch 1:1) was used for scanning and three-dimensional reconstruction. The CRHMSA of the extensor carpi radialis longus, extensor carpi radialis brevis, extensor digitorum, extensor digiti minimi, extensor carpi ulnaris, abductor pollicis longus, extensor pollicis brevis, extensor pollicis longus, extensor indicis and supinator were numbered as CRHMSA₁ through CRHMSA₁₀. The projection point of each CRHMSA on the body surface was defined as the puncture point (point P), and recorded as P₁ to P₁₀.

In the Syngo system (Siemens, Germany), the total length of the H and L lines were measured on the cross-sectional and coronal planes close to the skin using a curve measurement tool. The intersection points with H and L lines are defined as P_H (P_{1H}-P_{10H}) and P_L (P_{1L}-P_{10L}). The lengths from point a to P_H and P_L were measured and recorded as H' (H₁'-H₁₀') and L' (L₁'-L₁₀'). By calculating H'/H×100 % and L'/L×100 %, the percentage position of point P in the body surface coordinate system was determined. On the cross section, the line between point P and deep CRHMSA was projected to the skin in reverse direction, which was recorded as point P' (P₁'-P₁₀'). The depth from point P to CRHMSA (P-CRHMSA) and the length from point P to point P' (PP') were measured. The percentage depth of CRHMSA was determined by calculating P-CRHMSA/PP'×100 %.

Statistical analysis. To eliminate individual variations, all measurement data was converted into their own percentage ($x \pm S$, %). SPSS 21.0 software (IBM, USA) was used for statistical analysis: paired t-test was used for comparison between the left and right sides; the independent sample t-test was used for comparison between men and women; and one-way ANOVA was used for comparison of muscle spindle abundance among the upper, middle and lower parts of INDR. The test level is set to $\alpha = 0.05$.

RESULTS

Gross anatomy and Sihler's staining findings. The radial nerve is divided into superficial and deep terminal branches above the lateral epicondyle of humerus. The deep branch descends on the deep surface of the extensor carpi radialis brevis, and sends out several muscle branches before passing through the supinator. After the supinator muscle, the deep branch sends out remaining muscle branches (Fig. 1).

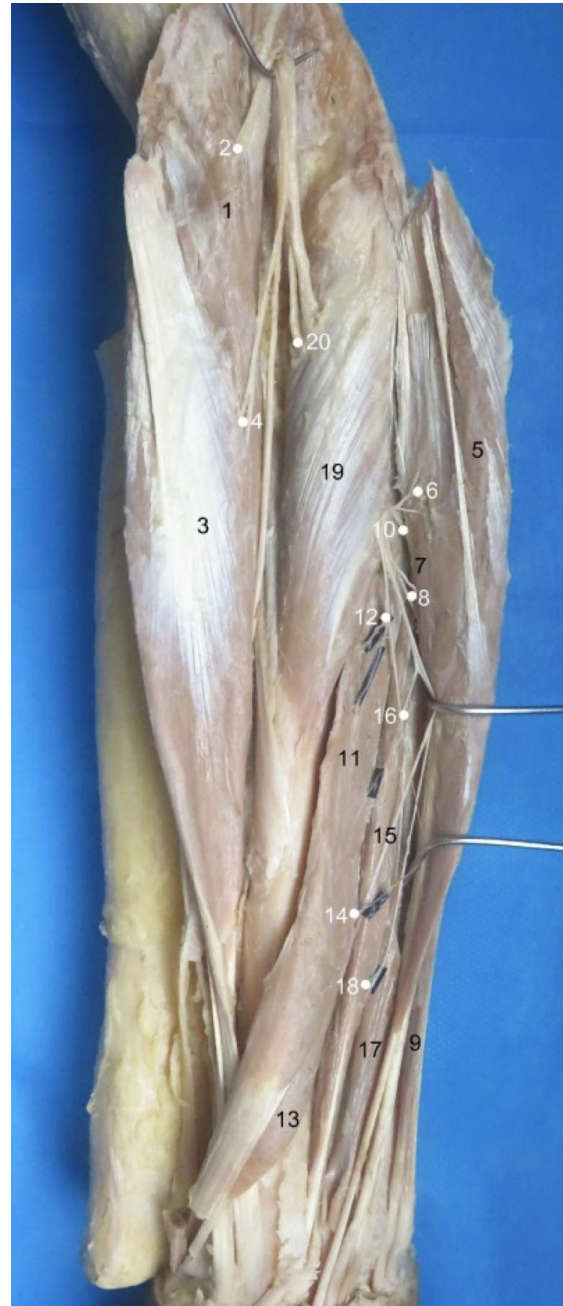


Fig. 1. Gross anatomy of the posterior forearm muscles innervation. 1 = extensor carpi radialis longus, 2 = extensor carpi radialis longus nerve entry point, 3 = extensor carpi radialis brevis, 4 = extensor carpi radialis brevis nerve entry point, 5 = extensor digitorum, 6 = extensor digitorum nerve entry point, 7 = extensor digiti minimi, 8 = extensor digiti minimi nerve entry point, 9 = extensor carpi ulnaris, 10 = extensor carpi ulnaris nerve entry point, 11 = abductor pollicis longus, 12 = abductor pollicis longus nerve entry point, 13 = extensor pollicis brevis, 14 = extensor pollicis brevis nerve entry point, 15 = extensor pollicis longus, 16 = extensor pollicis longus nerve entry point, 17 = extensor indicis, 18 = extensor indicis nerve entry point, 19 = supinator, 20 = supinator nerve entry point.

The nerve branch to the extensor carpi radialis longus is separated from the radial nerve trunk above the lateral epicondyle of the humerus and enters the muscle in the upper part on medial side of the muscle (Fig. 1). After the nerve entered the muscle, it was divided into two primary nerve branches, and then the branch-like branches formed a nerve intensive area (INDR₁) with an area of about (3.47±0.67) cm² at the level of (36.19±0.88) % to (52.90±0.64) % of the muscle belly length (Fig. 2).

The nerve branch to the extensor carpi radialis brevis is issued from the deep branch of the radial nerve below the lateral epicondyle of the humerus, and enters the muscle deep in the center of the upper muscle belly (Fig. 1). After entering the muscle, it is often divided into two primary nerve branches. The dendritic branches form a nerve dense region (INDR₂) with an area of about (4.25±0.29) cm² at the level of (30.56±0.35) % to (52.41±0.33) % of the muscle belly length (Fig. 2).

The nerve branch of the extensor digitorum muscle is issued from the deep branch of the radial nerve through the supinator muscle and enters the muscle in the middle of the superficial surface of the muscle (Fig. 1). After entering the muscle, it is often divided into three primary nerve branches. The dendritic branches form an area of (2.24±0.18) cm² nerve dense area (INDR₃) at the level of (20.54±0.30) % to (39.60±0.32) % of the length of the muscle belly (Fig. 3).

The nerve branch of the extensor digitorum minimi is issued from the deep branch of the radial nerve through the supinator muscle and enters the muscle at the upper part of the muscle belly (Fig. 1). After the nerve enters the muscle, the branches at all levels form a nerve dense area (INDR₄) with an area of about (0.46±0.08) cm² at the level of (39.37±0.26) % to (52.43±0.25) % of the muscle belly length (Fig. 3).

The nerve branch of the extensor carpi ulnaris is issued after the deep branch of the radial nerve passes through the supinator muscle, and enters the muscle at the 1/3 deep surface of the proximal muscle belly (Fig. 1). After entering the muscle, it is divided into two branches, which are on the ulnar and radial sides of the muscle respectively to the distal end of the muscle. Their dendritic branches form a nerve-dense area (INDR₅) with an area of about (4.14±0.22) cm² at the level of (22.22±0.63) % to (40.16±0.55) % of the nerve dense region (INDR₅) (Fig. 3).

The abductor pollicis longus nerve branch is a branch of the posterior interosseous nerve, which enters the muscle on the surface of the initial part of the muscle (Fig. 1). Three primary branches appear after the nerve enters the muscle and all sent out many dendritic branches in the middle of the muscle belly communicating with each other, forming a nerve intensive area (INDR₆) with an area of about (5.73±0.47) cm² at the level of (25.18±0.30) % to (44.90±0.27) % of the muscle belly length (Fig. 4).

The nerve branch to the extensor pollicis brevis is originates

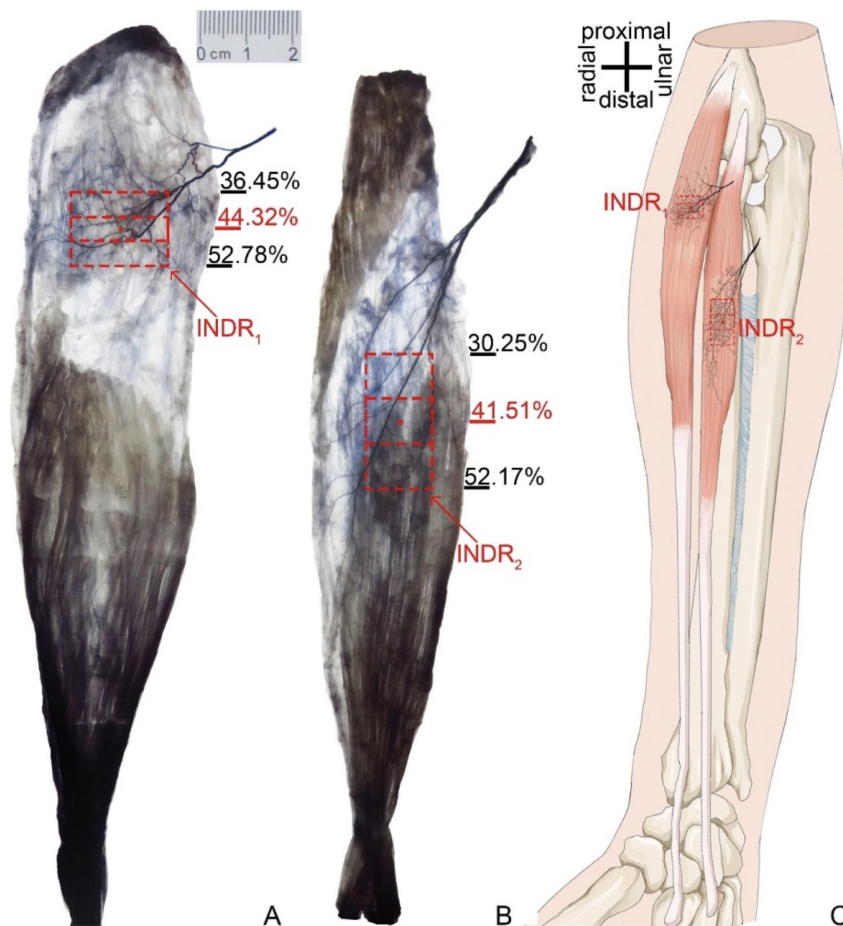


Fig. 2. Sihler's staining of extensor carpi radialis longus and extensor carpi radialis brevis. **A** and **B**: Sihler's staining of extensor carpi radialis longus and extensor carpi radialis brevis. Scale bar, cm. The red box represents INDR. The red dot represents the CRHMSAs. **C**: Schematic diagram of A and B.

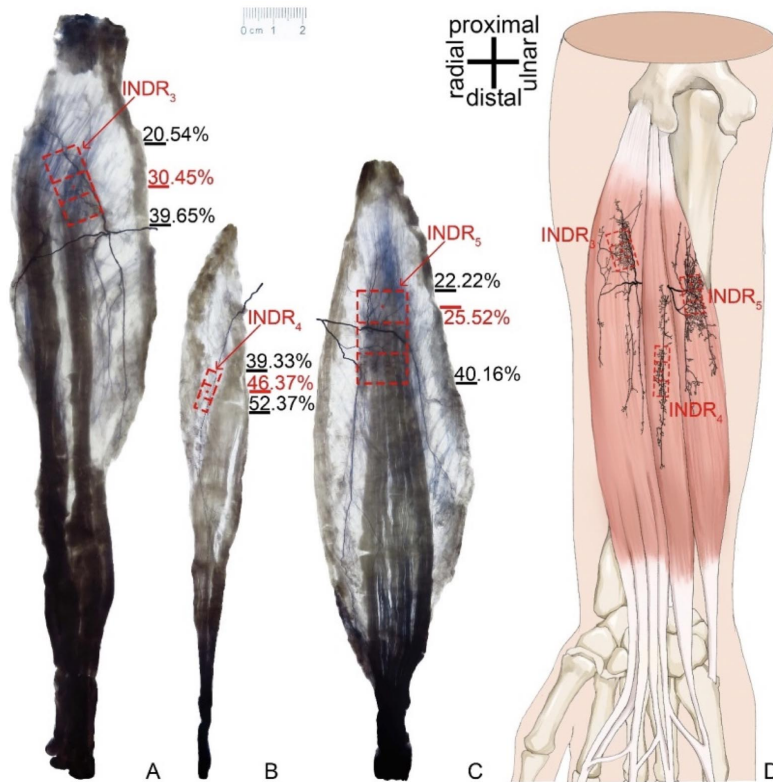


Fig. 3. Sihler's staining of extensor digitorum, extensor digiti minimi and extensor carpi ulnaris. A-C: Sihler's staining of extensor digitorum, extensor digiti minimi and extensor carpi ulnaris. Scale bar, cm. The red box represents INDR. The red dot represents the CRHMSAs. D: Schematic diagram of A-C.

from the posterior interosseous nerve and enters the muscle on the surface of the proximal 1/3 of the muscle belly (Fig. 1). The branches of the nerve, after entering the muscle, are denser in the upper part of the muscle, forming a nerve dense area (INDR₇) with an area of about (0.64±0.05) cm² at the level of (17.54±0.62) % to (42.36±0.48) % of the muscle belly length (Fig. 4).

After the nerve branch to the extensor pollicis longus is separated from the posterior interosseous nerve, it enters the muscle on the surface of the proximal 1/3 of the muscle belly (Fig. 1). After entering the muscle, the nerve first issues 3-5 primary branches, and then dendritic branches, forming a nerve-intensive area (INDR₈) with an area of about (1.13±0.11) cm² at the level of (46.67±0.71) % to (64.56±0.77) % of the muscle belly length (Fig. 4).

The extensor indicis branch comes from the posterior interosseous nerve and enters the muscle on the surface of the muscle origin (Fig. 1). The two primary branches sent out after the nerve entered the muscle, and the nerve branches in the muscle belly are dense and communicated with each other. At the level of (32.12±0.53) % to

(75.84±0.55) % of the muscle belly length, a nerve intensive area (INDR₉) with an area of about (1.87±0.13) cm² is formed (Fig. 4).

The nerve branch of the supinator comes off from the deep branch of the radial nerve and enters the muscle on the surface of the muscle origin (Fig. 1). Four primary nerve branches are formed after the nerve enters the muscle. The branches mainly form a nerve-dense area (INDR₁₀) with an area of about (4.79±0.22) cm² at the level of (26.15±0.45) % to (62.05±0.28) % of the muscle belly length (Fig. 5).

Comparison of muscle spindle abundance.

In the cross section of H&E staining, the muscle spindle capsule and the intrafusal fibers were red and the nucleus was blue (Fig. 6). The abundance of muscle spindles in the upper, middle and lower INDR of each muscle is different, as shown in Table I. The order of muscle spindle abundance of each muscle's INDR is: INDR₁₀, INDR₃, INDR₅, INDR₉, INDR₂, INDR₈, INDR₄, INDR₇, INDR₁, INDR₆ (Table I). The abundance of muscle spindles in the middle 1/3 of INDR₁, INDR₂, INDR₃, INDR₄, INDR₆, INDR₉ and INDR₁₀ is the highest. The abundance of muscle spindles in the upper 1/3 of INDR₅, INDR₇ and INDR₈ is the highest. There was no significant difference between the upper, middle and lower parts of INDR₄, INDR₈ and INDR₉ (P>0.05), and there was significant difference between the upper, middle and lower parts of INDR in other muscles (P>0.05). There is no significant difference between the left and right sides and between men and women (P>0.05) (Table II).

In the INDR of each muscle, the percentage of the center of the region of the highest muscle spindle abundance in the abdominal length was CRHMSA₁, (44.54±0.67) %; CRHMSA₂, (41.48±0.30) %; CRHMSA₃, (30.07±0.18) %; CRHMSA₄, (45.90±0.23) %; CRHMSA₅, (25.21±0.61) %; CRHMSA₆, (28.47±0.25) %; CRHMSA₇, (21.68±0.58) %; CRHMSA₈, (55.62±0.70) %; CRHMSA₉, (53.98±0.39) %; CRHMSA₁₀, (44.10±0.18) %.

Spiral CT localization of CRHMSA. The body surface projection points (P₁ and P₂) of CRHMSA₁ and CRHMSA₂ are located in the anterior forearm (Fig.7A1); the body surface projection points of CRHMSA₃, CRHMSA₄, CRHMSA₅, CRHMSA₆, CRHMSA₇, CRHMSA₈, CRHMSA₉ and CRHMSA₁₀ (P₃, P₄, P₅, P₆, P₇, P₈, P₉ and P₁₀)

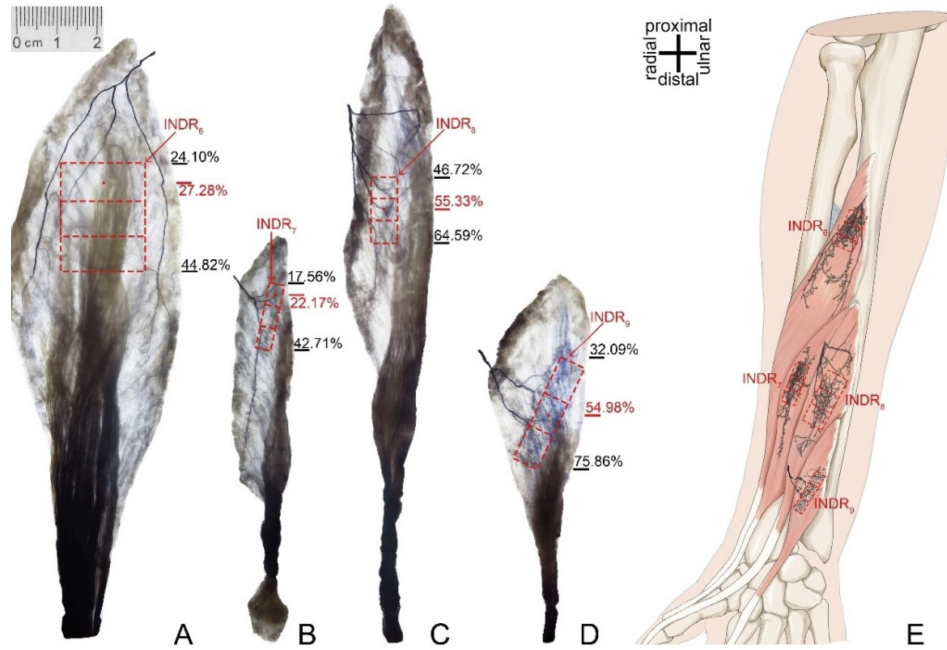


Fig. 4. Sihler's staining of abductor pollicis longus, extensor pollicis brevis, extensor pollicis longus and extensor indicis. **A-D**: Sihler's staining of abductor pollicis longus, extensor pollicis brevis, extensor pollicis longus and extensor indicis. Scale bar, cm. The red box represents INDR. The red dot represents the CRHMSAs. **E**: Schematic diagram of A-D.

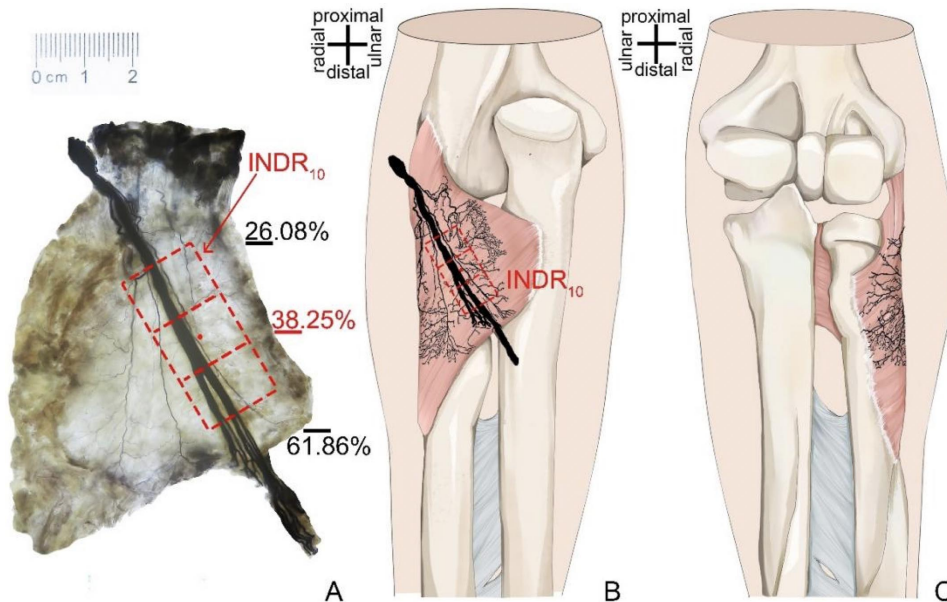


Fig. 5. Sihler's staining of supinator muscle. **A**: Sihler's staining of the supinator muscle. Scale bar, cm. The red box represents INDR. The red dot represents the CRHMSAs. **B**: Schematic diagram (rear view). **C**: Schematic diagram (front view). Each muscle branch has no blood vessels accompanying into the muscle.

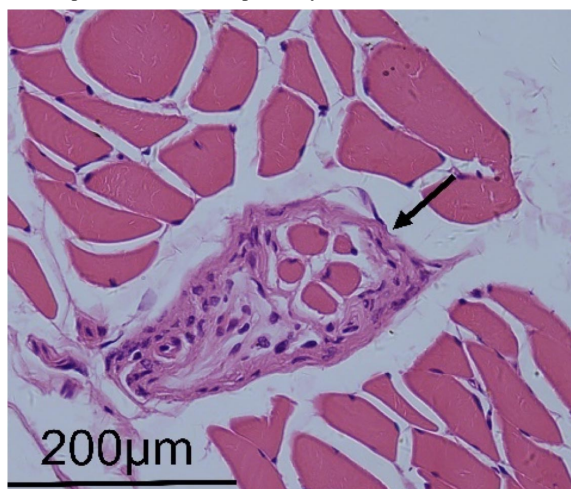
are located in the posterior forearm (Fig.7A2). The position of PH and PL of each CRHMSA in the posterior forearm muscles on the H and L lines and the depth of CRHMSA are shown in Table III. The data shows no significant difference

between men and women and between left and right sides ($P>0.05$). (Tables IV and V) This article uses the spiral CT positioning image of the extensor pollicis brevis as an example (Fig.7).

Table I. Comparison of muscle spindle abundance between the upper, middle and lower parts of each INDR (n= 12, mean ± SD).

INDRs	Parts of INDR	Muscle weight (g)	Actual number of muscle spindles	Predicted number of muscle spindles	Relative muscle spindle abundance
INDR ₁	Upper	1.04±0.03	15.83±0.90	20.88±0.32	0.76±0.04*
	Middle	0.99±0.09	16.50±0.96	20.33±0.90	0.81±0.05
	Lower	1.01±0.07	14.17±0.99	20.61±0.69	0.69±0.05*
INDR ₂	Upper	1.25±0.05	21.58±1.32	22.83±0.43	0.95±0.07△
	Middle	1.17±0.06	25.83±0.80	22.11±0.60	1.17±0.03
	Lower	1.00±0.06	20.83±1.52	20.45±0.66	1.02±0.07△
INDR ₃	Upper	0.41±0.03	16.17±1.28	13.26±0.50	1.22±0.10▽
	Middle	0.48±0.06	21.50±1.55	14.31±0.94	1.51±0.13
	Lower	0.50±0.06	16.08±1.44	14.56±0.90	1.11±0.12▽
INDR ₄	Upper	0.18±0.03	8.00±0.71	8.69±0.80	0.93±0.13☆
	Middle	0.10±0.03	7.08±0.64	6.64±0.95	1.08±0.14
	Lower	0.12±0.03	7.25±0.60	7.07±0.92	1.04±0.17☆
INDR ₅	Upper	0.58±0.04	21.83±0.99	15.72±0.53	1.39±0.07
	Middle	0.67±0.05	20.42±1.61	16.86±0.62	1.21±0.10▲
	Lower	0.73±0.04	20.25±1.16	17.56±0.51	1.15±0.08▲
INDR ₆	Upper	0.33±0.04	9.42±0.86	11.87±0.74	0.79±0.07★
	Middle	0.36±0.06	9.83±0.90	12.32±1.07	0.80±0.07
	Lower	0.33±0.05	9.33±1.49	11.80±0.89	0.71±0.13★
INDR ₇	Upper	0.17±0.03	8.00±1.08	8.47±0.70	0.95±0.14
	Middle	0.16±0.02	4.42±0.86	8.34±0.43	0.53±0.10○
	Lower	0.10±0.02	5.08±0.86	6.50±0.81	0.79±0.15○
INDR ₈	Upper	0.16±0.03	9.17±1.21	8.37±0.66	1.10±0.14
	Middle	0.15±0.03	8.83±0.80	8.13±0.71	1.09±0.13●
	Lower	0.15±0.03	8.75±0.72	8.09±0.87	1.09±0.13●
INDR ₉	Upper	0.31±0.02	14.67±0.94	11.46±0.47	1.28±0.10▼
	Middle	0.43±0.04	18.17±1.14	13.56±0.54	1.34±0.11
	Lower	0.32±0.04	15.58±0.76	11.74±0.63	1.33±0.06▼
INDR ₁₀	Upper	0.38±0.06	20.50±1.12	12.74±0.95	1.62±0.13■
	Middle	0.35±0.05	21.58±1.89	12.28±0.91	1.76±0.15
	Lower	0.21±0.02	15.25±1.30	9.55±0.50	1.60±0.16■

Note: INDR1 through INDR10 correspond to the intramuscular nerve-dense region within the following muscles: the extensor carpi radialis longus, extensor carpi radialis brevis, extensor digitorum, extensor digiti minimi, extensor carpi ulnaris, abductor pollicis longus, extensor pollicis longus, extensor pollicis brevis, extensor pollicis longus, extensor indicis and supinator. *, △, ▽, □, ▲, ♪, ○, ●, ▼, ■: Comparisons with the middle part of INDR1, middle part of INDR2, middle part of INDR3, middle part of INDR4, upper part of INDR5, middle part of INDR6, upper part of INDR7, upper part of INDR8, middle part of INDR9, and middle part of INDR10, respectively, P< 0.05.



DISCUSSION

Research significance and necessity. BoNT injection is a common method for the treatment of spastic limbs after stroke, lateral epicondylitis and dystonia (Galván Ruiz *et al.*, 2019; Dressler *et al.*, 2021; Schnitzler *et al.*, 2022; Motavasseli *et al.*, 2024; Poenaru *et al.*, 2024). However, injection with improper dose and position may lead to a decrease of muscle strength or atrophy of the non-targeted muscles. Although previous studies have anatomically located the nerve branches in the posterior forearm muscles (Jariwala *et al.*, 2014; Hackl *et al.*, 2015), the site of BoNT action was not involved. In this study, based on the relationship between intramuscular nerve and muscle spindle

Fig. 6. H&E staining of muscle spindles. Scale, 200 µm.

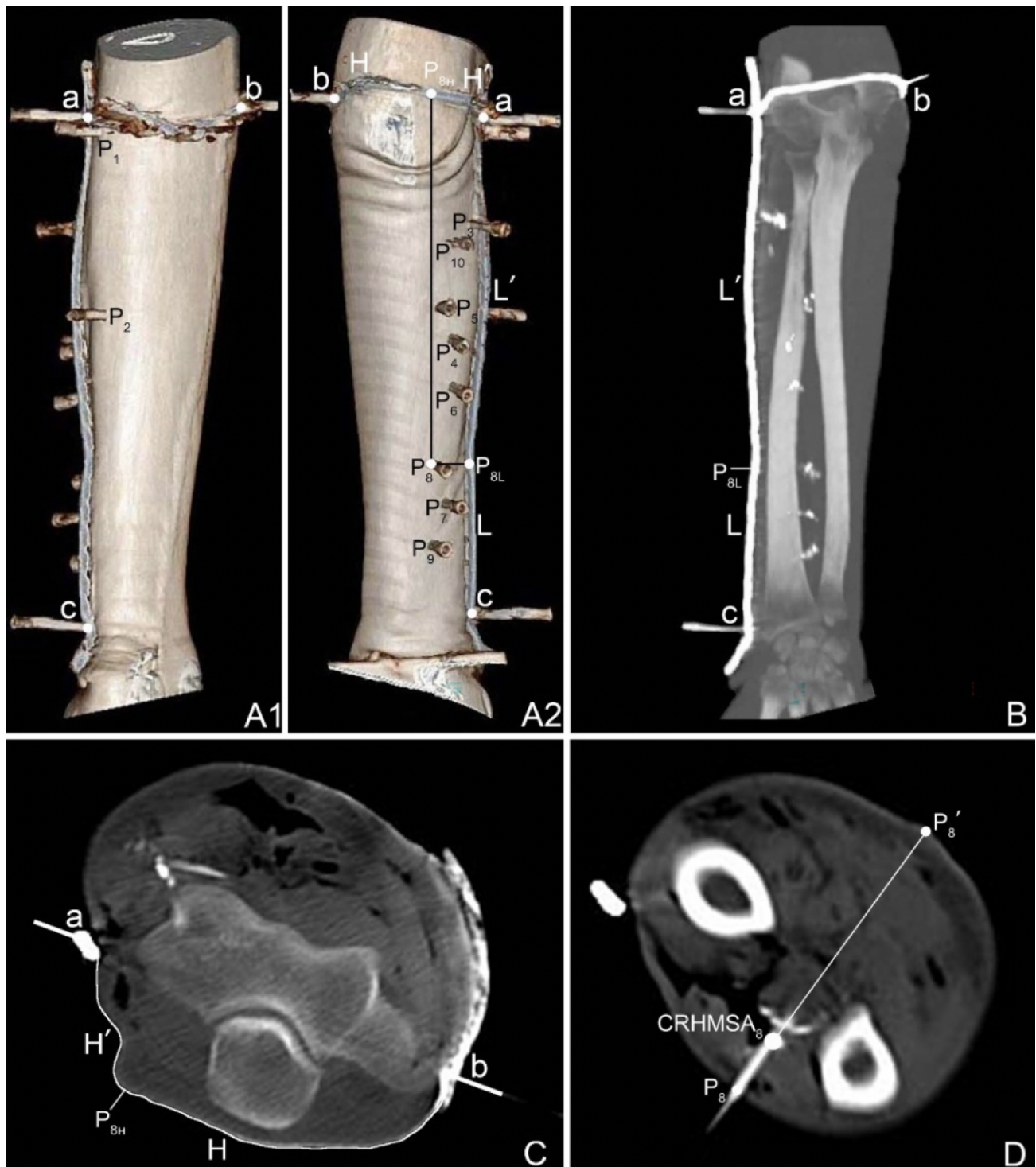


Fig. 7. Spiral CT localisation image of the CHRMSA of the extensor pollicis brevis muscle. A: Spiral CT localization image showing the position of each CHRMSA of the anterior forearm muscles on the body surface and the designed reference line. (A1) anterior forearm, (A2) posterior forearm. a=lateral epicondyle of the humerus; b=medial epicondyle of the humerus; c=radius styloid process. P8=the body surface projection point of the CHRMSA of the extensor pollicis brevis muscle. P8H=the intersection of the vertical line through P8 and the H line. P8L=the intersection of the horizontal line through P8 and the L line. a-P8H=H', a-P8L=L'. B: Measurement of the length of the L and L' lines on the coronal section. C: Measurement of the lengths of the H and H' lines on the cross section. D: Measurement of the depth of CHRMSA8 on the cross section.

Table II. Comparison of spindle abundance of each part of the INDR between left and right sides and between males and females (mean±SD).

NDRs	Parts of INDR	Muscle spindle abundance							
		Left side (n=12)	Right side (n=12)	t	P	Men (n=6)	Women (n=6)	t	P
INDR ₁	Upper	0.75±0.03	0.76±0.06	-0.315	0.759	0.77±0.04	0.75±0.05	0.706	0.496
	Middle	0.80±0.05	0.82±0.06	-0.614	0.553	0.83±0.06	0.80±0.05	0.943	0.368
	Lower	0.70±0.06	0.68±0.04	0.575	0.578	0.69±0.05	0.69±0.05	-0.113	0.912
INDR ₂	Upper	0.95±0.05	0.94±0.09	0.347	0.743	0.95±0.05	0.94±0.09	0.282	0.784
	Middle	1.17±0.03	1.17±0.04	-0.168	0.873	1.17±0.04	1.17±0.03	0.385	0.709
	Lower	1.00±0.07	1.04±0.07	-0.966	0.378	1.01±0.08	1.03±0.06	-0.581	0.574
INDR ₃	Upper	1.20±0.11	1.24±0.11	-0.542	0.600	1.20±0.13	1.24±0.08	-0.598	0.563
	Middle	1.50±0.14	1.52±0.13	-0.294	0.775	1.46±0.10	1.55±0.15	-1.209	0.254
	Lower	1.16±0.15	1.06±0.07	1.630	0.134	1.11±0.14	1.11±0.11	-0.112	0.913
INDR ₄	Upper	0.92±0.12	0.94±0.16	-0.225	0.827	0.94±0.16	0.92±0.12	0.349	0.735
	Middle	1.09±0.06	1.08±0.21	0.131	0.898	1.10±0.14	1.07±0.16	0.320	0.756
	Lower	1.01±0.08	1.09±0.24	-0.730	0.493	1.07±0.12	1.02±0.23	0.501	0.627
INDR ₅	Upper	1.39±0.07	1.40±0.09	-0.178	0.862	1.41±0.05	1.37±0.10	0.767	0.461
	Middle	1.24±0.11	1.19±0.11	0.739	0.477	1.17±0.07	1.25±0.13	-1.340	0.210
	Lower	1.17±0.09	1.14±0.09	0.485	0.638	1.18±0.09	1.13±0.08	0.898	0.391
INDR ₆	Upper	0.80±0.07	0.79±0.07	0.198	0.847	0.82±0.05	0.77±0.08	1.433	0.188
	Middle	0.82±0.06	0.79±0.09	0.647	0.516	0.81±0.06	0.79±0.09	0.294	0.775
	Lower	0.75±0.13	0.68±0.14	0.909	0.385	0.73±0.08	0.69±0.17	0.593	0.572
INDR ₇	Upper	0.97±0.08	0.93±0.21	0.383	0.717	0.94±0.19	0.97±0.11	-0.314	0.760
	Middle	0.58±0.07	0.48±0.12	1.575	0.176	0.56±0.05	0.50±0.14	0.939	0.381
	Lower	0.81±0.07	0.77±0.22	0.393	0.711	0.75±0.20	0.84±0.10	-0.995	0.343
INDR ₈	Upper	1.08±0.08	1.12±0.21	-0.459	0.665	1.12±0.12	1.08±0.19	0.353	0.731
	Middle	1.07±0.09	1.12±0.18	-0.529	0.620	1.07±0.13	1.12±0.15	-0.513	0.619
	Lower	1.05±0.13	1.13±0.15	-1.071	0.333	1.11±0.13	1.08±0.15	0.384	0.709
INDR ₉	Upper	1.25±0.04	1.31±0.15	-1.073	0.332	1.24±0.06	1.33±0.13	-1.514	0.161
	Middle	1.39±0.06	1.30±0.13	1.985	0.104	1.33±0.10	1.36±0.12	-0.563	0.586
	Lower	1.31±0.05	1.35±0.06	-1.281	0.256	1.34±0.07	1.32±0.05	0.682	0.511
INDR ₁₀	Upper	1.63±0.18	1.61±0.11	0.196	0.848	1.60±0.18	1.64±0.11	-0.557	0.590
	Middle	1.82±0.19	1.71±0.08	1.305	0.221	1.76±0.18	1.77±0.13	-0.126	0.902
	Lower	1.62±0.18	1.59±0.18	0.322	0.754	1.63±0.12	1.58±0.22	0.452	0.661

Table III. P_L and P_H positions on the L and H lines and the depth of CRHMSA (mean±SD).

CRHMSAs	P _H on line H(%) H'/H (%)	P _L on line L(%) L'/L (%)	Depth of CRHMSA(%) P-CRHMSA/PP'(%)
CRHMSA ₁	14.67±1.06	3.45±0.65	9.67±0.50
CRHMSA ₂	19.61±0.86	39.50±0.61	6.52±0.48
CRHMSA ₃	10.66±0.82	21.61±0.46	13.62±0.46
CRHMSA ₄	37.56±0.76	44.20±0.74	10.35±0.47
CRHMSA ₅	45.86±0.59	37.67±0.65	12.65±0.41
CRHMSA ₆	25.75 ±0.71	53.88±1.10	30.48±0.34
CRHMSA ₇	33.40±0.96	77.51±1.40	16.21±0.49
CRHMSA ₈	50.80±0.64	69.46±0.86	28.44±0.36
CRHMSA ₉	48.48±0.95	86.39±0.55	14.99±0.47
CRHMSA ₁₀	39.51±0.73	25.74±0.56	22.45±0.58

Note: INDR1 through INDR10 correspond to the intramuscular nerve-dense region within the following muscles: the extensor carpi radialis longus, extensor carpi radialis brevis, extensor digitorum, extensor digiti minimi, extensor carpi ulnaris, abductor pollicis longus, extensor pollicis brevis, extensor pollicis longus, extensor indicis and supinator.

Table IV. Comparison of the P and P positions on the H and L lines and the depth of CRHMSAs between the left and right sides(mean±SD).

CRHMSAs	P _H on line H(%)				P _L on line L(%)				Depth of CRHMSA(%)					
	Left side (n=12)		Right side (n=12)		Left side (n=12)		Right side (n=12)		Left side (n=12)		Right side (n=12)		P	
	Men (n=6)	Women (n=6)	t	P	Men (n=6)	Women (n=6)	t	P	Men (n=6)	Women (n=6)	t	P	Men (n=6)	Women (n=6)
CRHMSA ₁	14.68±1.12	14.66±1.11	0.040	0.970	3.39±0.59	3.50±0.75	-0.212	0.840	9.61±0.37	9.73±0.64	-0.388	0.714	6.46±0.51	6.58±0.49
CRHMSA ₂	19.65±0.72	19.58±1.05	0.146	0.890	39.62±0.67	39.39±0.59	0.797	0.461	13.77±0.40	13.47±0.49	1.228	0.274	10.57±0.40	10.12±0.45
CRHMSA ₃	10.68±0.86	10.64±0.87	0.063	0.952	21.56±0.48	21.67±0.47	-0.467	0.660	12.65±0.39	12.66±0.47	-0.067	0.949	16.33±0.61	16.09±0.36
CRHMSA ₄	37.70±0.82	37.43±0.74	0.506	0.634	44.35±0.70	44.05±0.81	0.850	0.434	28.43±0.37	28.45±0.39	-0.086	0.935	14.95±0.50	15.03±0.50
CRHMSA ₅	45.73±0.58	46.00±0.62	-0.895	0.412	37.58±0.51	37.76±0.81	-0.983	0.371	22.46±0.59	22.44±0.62	0.072	0.945	10.31±0.33	10.31±0.33
CRHMSA ₆	25.74±0.56	25.77±0.89	-0.058	0.956	53.92±1.00	53.83±1.29	0.113	0.914	30.50±0.37	30.50±0.37	-0.206	0.845	16.09±0.36	16.09±0.36
CRHMSA ₇	33.38±1.13	33.43±0.87	-0.084	0.937	77.61±1.54	77.41±1.39	0.198	0.851	16.33±0.61	16.09±0.36	0.989	0.368	14.95±0.50	15.03±0.50
CRHMSA ₈	50.76±0.58	51.00±0.78	-0.539	0.613	69.46±1.04	69.46±0.73	-0.033	0.975	28.43±0.37	28.45±0.39	-0.086	0.935	10.31±0.33	10.31±0.33
CRHMSA ₉	48.80±1.10	48.17±0.74	0.876	0.421	86.36±0.49	86.42±0.64	-0.268	0.799	22.46±0.59	22.44±0.62	0.072	0.945	10.31±0.33	10.31±0.33
CRHMSA ₁₀	39.55±0.86	39.47±0.66	0.249	0.813	25.64±0.57	25.84±0.58	-0.521	0.624	10.00±0.40	9.79±0.60	-0.782	0.453	6.46±0.51	6.58±0.49

Table V. Comparison of the P and P positions on the H and L lines and the depth of CRHMSAs between males and females (mean±SD).

CRHMSAs	P _H on line H(%)				P _L on line L(%)				Depth of CRHMSA(%)					
	Men (n=6)		Women (n=6)		Men (n=6)		Women (n=6)		Men (n=6)		Women (n=6)		P	
	Men (n=6)	Women (n=6)	t	P	Men (n=6)	Women (n=6)	t	P	Men (n=6)	Women (n=6)	t	P	Men (n=6)	Women (n=6)
CRHMSA ₁	14.25±1.07	15.09±1.00	-1.418	0.186	3.52±0.41	3.37±0.86	0.386	0.711	10.00±0.40	9.79±0.60	-0.782	0.453	6.46±0.51	6.58±0.49
CRHMSA ₂	19.52±0.76	19.71±1.01	-0.374	0.716	39.55±0.50	39.46±0.76	0.266	0.796	13.87±0.38	13.37±0.41	2.185	0.054	10.31±0.33	10.31±0.33
CRHMSA ₃	10.65±1.00	10.66±0.72	-0.013	0.990	21.45±0.40	21.78±0.49	-1.293	0.225	10.39±0.43	10.31±0.55	0.283	0.783	14.95±0.50	15.03±0.50
CRHMSA ₄	37.22±0.79	37.91±0.59	-1.721	0.116	44.47±0.64	43.92±0.78	1.339	0.210	12.51±0.32	12.80±0.46	-1.256	0.238	30.62±0.33	30.34±0.33
CRHMSA ₅	45.63±0.63	46.09±0.49	-1.399	0.192	37.72±0.32	37.62±0.91	0.262	0.802	16.41±0.58	16.00±0.31	1.541	0.154	16.09±0.36	16.09±0.36
CRHMSA ₆	25.85±0.85	25.66±0.60	0.448	0.664	53.98±1.27	53.78±1.02	0.293	0.775	28.50±0.33	28.37±0.41	0.618	0.550	15.00±0.28	15.00±0.28
CRHMSA ₇	33.77±0.77	33.03±1.05	1.400	0.192	77.46±1.73	77.57±1.15	-0.130	0.899	22.27±0.65	22.63±0.49	-1.084	0.304	10.31±0.33	10.31±0.33
CRHMSA ₈	51.09±0.64	50.67±0.68	1.095	0.299	69.51±0.78	69.41±1.00	0.203	-0.843	15.00±0.64	15.00±0.28	-0.017	0.987	10.31±0.33	10.31±0.33
CRHMSA ₉	48.32±0.65	48.64±1.23	-0.562	0.586	86.25±0.47	86.53±0.63	-0.881	0.399	10.00±0.40	9.79±0.60	-0.782	0.453	6.46±0.51	6.58±0.49
CRHMSA ₁₀	39.86±0.64	39.16±0.69	1.842	0.095	25.67±0.67	25.80±0.48	-0.372	0.717	10.00±0.40	9.79±0.60	-0.782	0.453	6.46±0.51	6.58±0.49

distribution, the center of the region of the highest muscle spindle abundance area in INDR was set as the best blocking target to achieve the surface percentage location and depth determination of CRHMSA. This localization strategy is expected to reduce the quantity of BoNT usage and the frequency of BoNT treatments. As a result, the risk of motor function damage is reduced, which is an important clinical value for patients (such as artists and programmers) who rely on fine muscle functions of the hand (Farinha Caroco *et al.*, 2024).

Characteristics of innervation.

The sources of nerve branch innervation of the posterior forearm muscle are diverse: the extensor carpi radialis longus branch is constantly located above the lateral epicondyles of the humerus; the starting point of the extensor carpi radialis brevis branch varied greatly; the supinator branch may originate from the radial nerve trunk or deep branch. After the radial nerve penetrates the supinator muscle, it sends out muscle branches such as extensor digitorum and extensor carpi ulnaris in subsequently (Genet *et al.*, 2012). Muscles with similar functions are often innervated by a common trunk, such as extensor digitorum and extensor digiti minimi, abductor pollicis longus and extensor pollicis brevis. Clarifying the rules of nerve entry points and branches can help guide the selection of BoNT targets and the functional reconstruction surgery after peripheral nerve injury.

Intramuscular nerve distribution pattern. Previous studies have shown that the nerve distribution pattern of posterior forearm muscle is closely related to muscle morphology: in flat or trapezoidal muscles, such as the supinator, nerve trunk runs perpendicular to the muscle fibers; in spindle muscles, nerve branch runs in parallel to muscle fiber; in multitendinous muscles, such as extensor digitorum, the nerve branch runs longitudinally and sends out recurrent branches (Lim *et al.*, 2004; Chen *et al.*, 2010). The purpose of this study is to clarify the location of INDR by Sihler's staining, which can not only improve the understanding of upper limb innervation, but also provide anatomical bases for the standardization of EMG detection sites, the design of bionic manipulator, and the treatment of muscle spasm by BoNT injection.

Distribution characteristics of muscle spindles. As a proprioceptor, the muscle spindle and its distribution is related to muscle function. The abundance of muscle spindles is higher in deep muscles than that in shallow muscles, and higher in small muscles than that in large muscles (Wang *et al.*, 2024). This study found that the high density of muscle spindles in the deeply located supinator muscle may be related to the need for fine motor regulation. In addition, this study also confirmed the phenomenon of muscle spindle uneven distribution, which is consistent with the theory of Banks (2006). From the results, we see that the highest abundance of muscle spindles are located in the upper part of INDR in the extensor carpi ulnaris and abductor pollicis longus, while the extensor carpi radialis longus and extensor digitorum are located in the middle. Since this study focused on the local INDR, the abundance of muscle spindles was generally higher than that of Banks' whole muscle data.

The best blocking target selection. The lesion associated with upper motor neurons leads to the de-inhibition of α -g neurons, the increase of muscle spindle sensitivity, and the aggravation of spasm. BoNT injection needs to maximize the blockade of intrafusal muscle fibers and minimize the impact on extrafusal muscle fibers (Phadke *et al.*, 2013). By positioning CRHMSA, this study provides an anatomical basis for the formulation of individualized injection plans, which is helpful to improve the efficacy and quality of rehabilitation.

Advantages and limitations. In this study, Sihler's staining, H&E staining, and spiral CT three-dimensional reconstruction technology were used to achieve accurate positioning of CRHMSA, which effectively improved the feasibility of clinical procedures. However, due to the limited sample size, it is still necessary to verify the universality of the method in a wider population in consideration of possible

impacts from racial and regional differences. In clinical practice, for deep muscle positioning, it is recommended to combine with ultrasound or electrical stimulation guidance to improve accuracy. In addition, it is necessary to further explore the relationship between the distribution of muscle spindles and the severity of spasm, in order to promote the development of individualized rehabilitation strategies.

ACKNOWLEDGMENTS

The authors would like to acknowledge Xufeng Tian for her excellent technical assistance in spiral CT scanning. The authors sincerely thank those who donated their bodies to science so that this anatomical research could be performed. Results from such research can potentially increase mankind's knowledge and improve patient care. Therefore, these donors and their families deserve our utmost gratitude. We are grateful for the support from the National Natural Science Foundation of China (No: 32260217) and the Science and Technology Key Project of Guizhou (No: ZK-2022-056) and the Guizhou University Student Innovation Program (No: S202310661176).

XIANG, L.; WU, X.; LIU, J.; LUO, D.; TAO, L.; ZHANG, M.X. & YANG, S. Localización de la región central de mayor abundancia de husos musculares en los músculos del compartimiento posterior del antebrazo para la inyección de toxina botulínica. *Int. J. Morphol.*, 44(2):562-573, 2026.

RESUMEN: Este estudio tuvo como objetivo definir los puntos y profundidades precisos de punción en la superficie corporal para la región central de mayor abundancia de husos musculares (CRHMSA) en los músculos del compartimiento posterior del antebrazo, con el fin de guiar las inyecciones de toxina botulínica. En un estudio con 24 cadáveres, se empleó la tinción de Sihler para los nervios intramusculares, la cuantificación histológica de los husos musculares y la tomografía computarizada para la localización de la CRHMSA. Las líneas de referencia incluyeron la horizontal (línea H, entre los epicóndilos humerales) y la longitudinal (línea L, desde el epicóndilo lateral hasta proceso estiloides del radio). La línea PP', que representa la profundidad de punción, se definió como la distancia entre las proyecciones cutáneas anterior (P) y posterior (P') del CRHMSA. El CRHMSA se ubicó en el medio de la región densa de nervios (INDR) para los músculos extensor radial largo del carpo, extensor radial corto del carpo, extensor de los dedos, extensor del dedo mínimo, abductor largo del pulgar, extensor del índice y supinador, y en la porción superior de la INDR para los músculos extensor ulnar del carpo, extensor corto del pulgar y extensor largo del pulgar. Las coordenadas de la línea H fueron 14,67 %, 19,61 %, 10,66 %, 37,56 %, 25,75 %, 48,48 %, 39,51 %, 45,86 %, 33,40 % y 50,80 %, respectivamente. Las coordenadas de la línea L fueron 3,45 %, 39,50 %, 21,61 %, 44,20 %, 53,88 %, 86,39 %, 25,74 %, 37,67 %, 77,51 % y 69,46 %, respectivamente. Las profundidades de punción fueron 9,67 %, 6,52 %, 13,62 %, 10,35 %, 30,48 %,

14,99 %, 22,45 %, 12,65 %, 16,21 % y 28,44 % de la línea PP', respectivamente. Estos hallazgos proporcionan una guía anatómica para mejorar la precisión de las inyecciones de toxina botulínica para el tratamiento de la espasticidad.

PALABRAS CLAVE: Músculos del compartimiento posterior del antebrazo; Nervio intramuscular; Abundancia de husos musculares; Toxina botulínica; Localización del objetivo.

REFERENCES

- Banks, R. W. An allometric analysis of the number of muscle spindles in mammalian skeletal muscles. *J. Anat.*, 208(6):753-68, 2006.
- Chen, G.; Jiang, H.; Liu, A.; Zhang, J.; Lin, Z.; Dang, R.; Yu, D.; Li, W. & Liu, B. Neurovascular details about forearm muscles: Applications in their clinical use in functional muscular transfer. *Surg. Radiol. Anat.*, 32(1):3-8, 2010.
- Dressler, D.; Altavista, M. C.; Altenmueller, E.; Bhidayasi, R.; Bohlega, S.; Chana, P.; Chung, T. M.; Colosimo, C.; Fheodoroff, K.; Garcia-Ruiz, P. J.; et al. Consensus guidelines for botulinum toxin therapy: General algorithms and dosing tables for dystonia and spasticity. *J. Neural Transm. (Vienna)*, 128(3):321-35, 2021.
- Facciorusso, S.; Spina, S.; Picelli, A.; Baricich, A.; Francisco, G. E.; Molteni, F.; Wissel, J. & Santamato A. The role of botulinum toxin type-A in spasticity: research trends from a bibliometric analysis. *Toxins (Basel)*, 16(4):184, 2024.
- Farinha Caroco, M. T.; Zão, A.; Ribeiro, J.; Fialho, A.; Milet, V. & Meira, B. Musician's dystonia in a percussionist - clinical video analysis and botulinum toxin intervention: a case report. *J. Rehabil. Med.*, 56:jrm34877, 2024.
- Galván Ruiz, A.; Vergara Díaz, G.; Rendón Fernández, B. & Echevarría Ruiz De Vargas, C. Effects of ultrasound-guided administration of botulinum toxin (IncobotulinumtoxinA) in patients with lateral epicondylitis. *Toxins (Basel)*, 11(1):46, 2019.
- Genet, F.; Autret, K.; Schnitzler, A.; Lautridou, C.; Bernuz, B.; Denormandie, P.; Allieu, Y. & Parratte, B. Motor branch of extensor carpi radialis longus: anatomic localization. *Arch. Phys. Med. Rehabil.*, 93(12):2309-12, 2012.
- Hackl, M.; Wegmann, K.; Lappen, S.; Helf, C.; Burkhart, K. J. & Müller, L. P. The course of the posterior interosseous nerve in relation to the proximal radius: Is there a reliable landmark? *Injury*, 46(4):687-92, 2015.
- Hesse, S.; Brandt-Hesse, B.; Bardeleben, A.; Werner, C. & Funk, M. Botulinum toxin A treatment of adult upper and lower limb spasticity. *Drugs Aging*, 18(4):255-62, 2001.
- Jariwala, A.; Krishnan, B.; Soames, R. & Wigderowitz, C. A. Important anatomical relationships of the posterior interosseous nerve in the distal forearm for surgical planning: A cadaveric study. *J. Wrist Surg.*, 3(1):60-3, 2014.
- Ji, S.; Luo, H.; Wen, S. & Yang, S. Localization of the center of intramuscular nerve dense regions in deltoid muscle: An applied anatomical study. *Int. J. Morphol.*, 43(5):1747-53, 2025.
- Kroumpouzou, G.; Kassir, M.; Gupta, M.; Patil, A. & Goldust, M. Complications of Botulinum toxin A: An update review. *J. Cosmet. Dermatol.*, 20(6):1585-90, 2021.
- Li, S.; Francisco, G. E. & Rymer, W. Z. A new definition of poststroke spasticity and the interference of spasticity with motor recovery from acute to chronic stages. *Neurorehabil. Neural Repair*, 35(7):601-10, 2021.
- Lim, A. Y. T.; Pereira, B. P.; Kumar, V. P.; De Coninck, C.; Taki, C.; Baudet, J. & Merle, M. Intramuscular innervation of upper-limb skeletal muscles. *Muscle Nerve*, 29(4):523-30, 2004.
- Mahrous, A.; Birch, D.; Heckman, C. J. & Tysseling, V. Muscle spasms after spinal cord injury stem from changes in motoneuron excitability and synaptic inhibition, not synaptic excitation. *J. Neurosci.*, 44(1):e1695232023, 2024.
- Motavasseli, D.; Delorme, C.; Bayle, N.; Gracies, J.-M.; Roze, E. & Baude, M. Use of botulinum toxin in upper-limb tremor: systematic review and perspectives. *Toxins (Basel)*, 16(9):392, 2024.
- Phadke, C. P.; On, A. Y.; Kirazli, Y.; Ismail, F. & Boulias, C. Intrafusal effects of botulinum toxin injections for spasticity: revisiting a previous paper. *Neurosci. Lett.*, 541:20-3, 2013.
- Poenaru, D.; Sandulescu, M. I.; Potcovaru, C.-G. & Cinteza, D. Botulinum toxin in chronic lateral epicondylitis, from tendon to muscle approach-A review. *Life (Basel)*, 14(4):528, 2024.
- Schnitzler, A.; Dince, C.; Freitag, A.; Iheanacho, I.; Fahrbach, K.; Lavoie, L.; Loze, J.-Y.; Forestier, A. & Gasq, D. AbobotulinumtoxinA doses in upper and lower limb spasticity: a systematic literature review. *Toxins (Basel)*, 14(11):734, 2022.
- Slawek, J.; Bogucki, A. & Reclawowicz, D. Botulinum toxin type A for upper limb spasticity following stroke: An open-label study with individualised, flexible injection regimens. *Neurol. Sci.*, 26(1):32-9, 2005.
- Therkildsen, E. R.; Kaster, P. & Nielsen, J. B. A scoping review on muscle cramps and spasms in upper motor neuron disorder-two sides of the same coin? *Front. Neurol.*, 15:1360521, 2024.
- Wang, D.; Chen, P.; Jia, F.; Wang, M.; Wu, J. & Yang, S. Division of neuromuscular compartments and localization of the center of the highest region of muscle spindles abundance in deep cervical muscles based on Sihler's staining. *Front. Neuroanat.*, 18:1340468, 2024.
- Wang, J.; Li, Y.; Wang, M. & Yang, S. Localization of the center of the intramuscular nerve dense region of the suboccipital muscles: An anatomical study. *Front. Neurol.*, 13:863446, 2022.
- Yu, J.; Li, Y.; Yang, L.; Li, Y.; Zhang, S. & Yang, S. The highest region of muscle spindle abundance should be the optimal target of botulinum toxin A injection to block muscle spasms in rats. *Front. Neurol.*, 14:1061849, 2023.
- Zhou, J.; Jia, F.; Chen, P.; Zhou, G.; Wang, M.; Wu, J. & Yang, S. Localisation of the centre of the highest region of muscle spindle abundance of anterior forearm muscles. *J. Anat.*, 244(5):803-14, 2024.

Corresponding author:
Ming Xiaoming Zhang, Professor
Center for Medical Education
Westlake University School of Medicine
18 Shilongshan Street
Hangzhou 310024
CHINA

E-mail: mxzhang@westlake.edu.cn

Corresponding author:
Shengbo Yang, Professor
Department of Anatomy
Xinpu New Developing District
Zunyi Medical University
6 West University Road
Zunyi 563099
CHINA

E-mail: yangshengbo8205486@163.com